

Ideal optomechanically induced transparency generation in a cavity optoelectromechanical system

Jing Wang(王婧) and Xue-Dong Tian(田雪冬)
Citation: Chin. Phys. B, 2021, 30 (**10**): 104211. DOI: 10.1088/1674-1056/ac1924
Journal homepage: http://cpb.iphy.ac.cn; http://iopscience.iop.org/cpb

What follows is a list of articles you may be interested in

Multiple induced transparency in a hybrid driven cavity optomechanical device with a two-level system

Wei Zhang(张伟), Li-Guo Qin(秦立国), Li-Jun Tian(田立君), and Zhong-Yang Wang(王中阳)
Chin. Phys. B, 2021, 30 (**9**): 094203. DOI: 10.1088/1674-1056/abf642

Quantum storage of single photons with unknown arrival time and pulse shapes

Yu You(由玉), Gong-Wei Lin(林功伟), Ling-Juan Feng(封玲娟), Yue-Ping Niu(钮月萍), and Shang-Qing Gong(龚尚庆)
Chin. Phys. B, 2021, 30 (**8**): 084207. DOI: 10.1088/1674-1056/abfbd3

Effective Hamiltonian of the Jaynes-Cummings model beyond rotating-wave approximation

Yi-Fan Wang(王伊凡), Hong-Hao Yin(尹洪浩), Ming-Yue Yang(杨明月), An-Chun Ji(纪安春), and Qing Sun(孙青)
Chin. Phys. B, 2021, 30 (**6**): 064204. DOI: 10.1088/1674-1056/abd930

Perfect photon absorption based on the optical parametric process

Yang Zhang(张旸), Yu-Bo Ma(马宇波), Xin-Ping Li(李新平), Yu Guo(郭钰), and Chang-Shui Yu(于长水)
Chin. Phys. B, 2021, 30 (**6**): 064203. DOI: 10.1088/1674-1056/abd7d9

Controlling multiple optomechanically induced transparency in the distant cavity-optomechanical system

Rui-Jie Xiao(肖瑞杰), Gui-Xia Pan(潘桂侠), and Xiao-Ming Xiu(修晓明)
Chin. Phys. B, 2021, 30 (**3**): 034209. DOI: 10.1088/1674-1056/abc7a4

Ideal optomechanically induced transparency generation in a cavity optoelectromechanical system*

Jing Wang(王婧)[1,2] and Xue-Dong Tian(田雪冬)[2,†]

[1] College of Physics, Tonghua Normal University, Tonghua 134000, China
[2] College of Physics Science and Technology, Guangxi Normal University, Guilin 541004, China

(Received 22 May 2021; revised manuscript received 14 July 2021; accepted manuscript online 30 July 2021)

The ideal optomechanically induced transparency effects of an output probe field are investigated in a cavity optoelectromechanical system, which is composed of an optical cavity, a charged mechanical resonator, and a charged object. Although the charged mechanical resonator damping rate is nonzero, the ideal optomechanically induced transparency can still appear due to the non-rotating wave approximation effect in the system. The location of optomechanically induced transparency dip can be controlled via the Coulomb coupling strength. In addition, we find that both the transparency window width and the maximum dispersion curve slope are closely related to the optical cavity decay rate.

Keywords: ideal optomechanically induced transparency, cavity optoelectromechanical system, transparency window width

PACS: 42.50.Pq, 42.50.Nn, 42.50.Ct **DOI:** 10.1088/1674-1056/ac1924

1. Introduction

Cavity optomechanical systems[1–38] have become one hot topic in the development of manipulating light. During the past decades, scientists have never stopped exploring, then a series of phenomena have been obtained one after the other in cavity optomechanical systems, for example, optomechanically induced transparency (OMIT),[4,5] entanglement,[8] ground-state cooling of the mechanical resonator,[9–11] optomechanically induced absorption,[7,12] amplification,[13] normal-mode splitting,[14] and Fano resonance.[15] A notable achievement discovered among these phenomena is OMIT, which has been first proposed theoretically in Ref. [4] and first experimental demonstrated in Ref. [5]. Subsequently, many significant new phenomena have been achieved base on OMIT, such as reversed OMIT,[17,18] nonlinear OMIT,[19] vector OMIT,[20] multiple OMIT,[15,21] higher-order OMIT,[22] and nonreciprocal OMIT.[23] These phenomena make cavity optomechanical system a powerful platform to realize light storage and delay[24,25] on account of the abnormal dispersion accompanied with a small width of the transparency window.[1,2] However, a practical problem is that it is very difficult to achieve both a large depth and narrow width of the transparency window in OMIT.[1,2] So, it is still a long-standing challenge to obviously improve OMIT. But recently Yan[1,2] studied ideal OMIT with the non-rotating wave approximation (NRWA) effect which was not considered in previous works. Compared with the traditional OMIT case, in which there still exists little residual absorption at the window centre, the idea OMIT means precise non-absorption indicating the unitary window depth at the window center. In addition, the width of the window is also narrow, so it is viable to achieve ideal transparency and the ultraslow light.

The conventional cavity optomechanical systems can be made up of one optical cavity, and one mechanical resonator. Most attention has been focused on the conventional cavity optomechanical system, but it is necessary to generalize it to different complex cavity optomechanical systems,[39–46] because that complex cavity optomechanical systems can exhibit more richer quantum behaviors. Complex cavity optomechanical systems include multi-mechanical resonator cavity optomechanical system,[39] cavity optoelectromechanical system,[40,42] atomic-medium assisted cavity optomechanical system,[16] multi-cavity optomechanical system with and without optical parametric amplifier,[44–46] and so on. In the complex cavity optomechanical systems, cavity optoelectromechanical system has attracted more attention, which is composed of a charged object and a cavity optomechanical system. In this system, Zhang *et al.*[42] has implemented the precise measurement of the charge number for small charged object via OMIT.

Although Zhang *et al.*[42] have proposed the scheme to realize precise measurement in cavity optoelectromechanical system, other output probe field properties of this system also attract our interest. In this work, inspired by the ideas in Refs. [1,2,42], we consider to explore the ideal OMIT properties in a cavity optoelectromechanical system with the NRWA effect. To our knowledge, the ideal OMIT considering the NRWA effect has not been studied in a cavity optoelectrome-

*Project supported by the Natural Science Foundation of Guangxi Province, China (Grant Nos. 2018GXNSFBA281003, 2019GXNSFAA245034, and AD19245180) and Science Fund of Tonghua Normal University (Grant No. 202017ND).

†Corresponding author. E-mail: snowtxd@mailbox.gxnu.edu.cn

© 2021 Chinese Physical Society and IOP Publishing Ltd

chanical system. Our work shows the ideal OMIT can be achieved via NRWA effect. With the appropriate parameter regime, we further consider the effect of the interaction between a charged mechanical resonator and a charged object with coulomb coupling strength, the cavity decay rate, and mechanical resonator damping rate on the ideal OMIT phenomenon. Firstly, the ideal OMIT phenomenon can be found in the resolved or unresolved sideband regime, respectively. Secondly, by increasing coulomb coupling strength, the location of the OMIT dip moves leftward significantly. Thirdly, the transparency window width of ideal OMIT is sensitive to the cavity decay rate, which is very important because cavity decay rate increases, transparency window width becomes narrower and does not affect the depth of the window. Fourthly, the maximum dispersion curve slope also depends on the cavity decay rate.

2. Model and equations

The cavity optoelectromechanical system considered in our work is presented schematically in Fig. 1, and the optical cavity is driven by a relatively strong driven field (frequency $\omega_{\rm L}$, strength $E_{\rm L}$) and a weak probe field (frequency $\omega_{\rm p}$, strength $E_{\rm p}$). The charged mechanical resonator $Q_{\rm b}$ (frequency $\omega_{\rm m}$, mass m, damping rate $\gamma_{\rm m}$, position q, momentum p, and charge $Q_{\rm b}$) is simultaneously coupled to the optical cavity (frequency $\omega_{\rm c}$) via radiation pressure and to the adjoining charged object $Q_{\rm d}$ (charge $Q_{\rm d}$) via the Coulomb force. So, there are two kinds of interaction in the cavity optoelectromechanical system, which include optomechanical coupling and the Coulomb interaction. In the absence of optomechanical coupling and the Coulomb interaction, the equilibrium separation from the charged object to the charged mechanical resonator is expressed by r_0. The Hamiltonian of the cavity optoelectromechanical system is given as[42]

$$\begin{aligned} H =\ & \hbar\omega_{\rm c}c^{\dagger}c+\left(\frac{p^2}{2m}+\frac{m\omega_{\rm m}^2}{2}q^2\right)-g_0c^{\dagger}cq \\ & -\frac{Q_{\rm b}Q_{\rm d}}{4\pi\varepsilon(r_0-q)}+{\rm i}\hbar E_{\rm L}(c^{\dagger}{\rm e}^{-{\rm i}\omega_{\rm L}t}-c{\rm e}^{{\rm i}\omega_{\rm L}t}) \\ & +{\rm i}\hbar(E_{\rm p}c^{\dagger}{\rm e}^{-{\rm i}\omega_{\rm p}t}-E_{\rm p}^{*}c{\rm e}^{{\rm i}\omega_{\rm p}t}). \end{aligned} \tag{1}$$

The first and second terms on the right-hand side of Eq. (1) present free Hamiltonian of the optical cavity, and the charged mechanical resonator, respectively. The annihilation operator c and creation operator $c^{\dagger}$ satisfy the commutation relation $\left[c,c^{\dagger}\right]=1$. The third term in Eq. (1) represents optomechanical interaction between the optical cavity and the charged mechanical resonator due to the radiation pressure with the optomechanical coupling strength g_0. The fourth term in Eq. (1) shows the Coulomb interaction of the charged mechanical resonator with charged object. As compared with the equilibrium separation r_0, the charged mechanical resonator position q is relatively small, i.e., $q\ll r_0$, so the term of Coulomb interaction between the charged mechanical resonator and charged object can be rewritten as $-\frac{Q_{\rm b}Q_{\rm d}}{4\pi\varepsilon(r_0-q)}=-\frac{Q_{\rm b}Q_{\rm d}}{4\pi\varepsilon r_0}(1+\frac{q}{r_0}+\frac{q^2}{r_0^2})$. In principle, the first two terms to the right-hand side of the above equation contribute small to the Coulomb interaction. For the convenience of analysis, the effect of the first two terms can be neglected. So the Coulomb interaction can be reduced to the simpler form ηq^2, where $\eta=\frac{Q_{\rm b}Q_{\rm d}}{4\pi\varepsilon r_0^3}$ is Coulomb coupling strength. In the case without Coulomb coupling strength η, i.e., $\eta=0$, the charged object is fully decoupled from the charged mechanical resonator, so the cavity optoelectromechanical system is reduced to the cavity optomechanical system. While whenever $\eta\neq 0$, the charged object, optical cavity, and charged mechanical resonator are all coupled. The last two terms in Eq. (1) correspond to the interaction between the optical cavity and the applied fields. The Hamiltonian in Eq. (1) in the rotating frame at the driven field frequency $\omega_{\rm L}$ can be presented as below:

$$\begin{aligned} H =\ & \hbar\Delta_{\rm c}c^{\dagger}c+\left(\frac{p^2}{2m}+\frac{m\omega_{\rm m}^2}{2}q^2\right)-g_0c^{\dagger}cq-\eta q^2 \\ & +{\rm i}\hbar E_{\rm L}(c^{\dagger}-c)+{\rm i}\hbar(E_{\rm p}c^{\dagger}{\rm e}^{-{\rm i}\delta t}-E_{\rm p}^{*}c{\rm e}^{{\rm i}\delta t}), \end{aligned} \tag{2}$$

where $\Delta_{\rm c}=\omega_{\rm c}-\omega_{\rm L}$, and $\delta=\omega_{\rm p}-\omega_{\rm L}$. Based on Eq. (2), the Langevin equations of the cavity optoelectromechanical system operators can be described as below:[47]

$$\begin{aligned} \dot{q} &= \frac{p}{m}, \\ \dot{p} &= -\frac{\gamma_{\rm m}}{2}p-m\omega_{\rm m}^2q+g_0c^{\dagger}c+2\eta q, \\ \dot{c} &= -2\kappa_{\rm c}c-{\rm i}\Delta_{\rm c}c+\frac{\rm i}{\hbar}g_0cq+E_{\rm L}+E_{\rm p}{\rm e}^{-{\rm i}\delta t}. \end{aligned} \tag{3}$$

Under the mean field approximation and using the factorization assumption, we write the Langevin equations for the mean values as below:

$$\begin{aligned} \langle\dot{q}\rangle &= \frac{\langle p\rangle}{m}, \\ \langle\dot{p}\rangle &= -\frac{\gamma_{\rm m}}{2}\langle p\rangle-m\omega_{\rm m}^2\langle q\rangle+g_0\langle c^{\dagger}\rangle\langle c\rangle+2\eta\langle q\rangle, \\ \langle\dot{c}\rangle &= -2\kappa_{\rm c}\langle c\rangle-{\rm i}\Delta_{\rm c}\langle c\rangle+\frac{\rm i}{\hbar}g_0\langle c\rangle\langle q\rangle+E_{\rm L}+E_{\rm p}{\rm e}^{-{\rm i}\delta t}. \end{aligned} \tag{4}$$

The driven field provides a steady-state mean value of the operator $A_{\rm s}$ ($A={\rm p,q,c}$), while the probe field causes a perturbation to the steady state. We suppose the operator A can be approximately written by using the following form:

$$\langle A\rangle=A_{\rm s}+E_{\rm p}\delta A_{+}{\rm e}^{-{\rm i}\delta t}+E_{\rm p}^{*}\delta A_{-}{\rm e}^{{\rm i}\delta t}. \tag{5}$$

Substituting Eq. (5) into Eq. (4), and setting $x=\delta-\omega_{\rm m}$, $\omega_{\rm m}\sim\delta\sim\Delta$, we can get the following analytical expressions:

$$\begin{aligned} p_{\rm s} &= 0, \\ q_{\rm s} &= \frac{g_0|c_{\rm s}|^2}{m\omega_{\rm m}^2-2\eta}, \\ c_{\rm s} &= \frac{E_{\rm L}}{2\kappa_{\rm c}+{\rm i}\Delta}, \end{aligned}$$

$$\delta c_+ = \frac{1}{2\kappa_c - ix + \dfrac{\beta}{\dfrac{\gamma_m}{4} - ix - \dfrac{i\eta}{m\omega_m} + N}}, \tag{6}$$

where $\Delta = \Delta_c - \frac{1}{\hbar} g_0 q_s$, and β and N are given as

$$\beta = \frac{g_0^2 |c_s|^2}{2\hbar m \omega_m}, \tag{7}$$

$$N = -\frac{\beta}{2\kappa_c - 2i\omega_m}. \tag{8}$$

From Eq. (6), we notice that the term N is very interesting. When we apply rotating wave approximation to solve the Langevin equations, the term N does not exist in δc_+ (see Appendix A for details). Hence we call the term N is NRWA effect.[1,2]

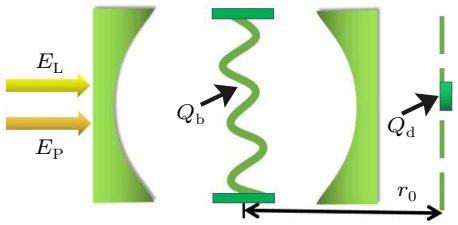


Fig. 1. Schematic diagram for the cavity optoelectromechanical system with one optical cavity, one charged mechanical resonator charges is Q_b, and one charged object charges is Q_d. The charged mechanical resonator is coupling to an adjoining charged object via the Coulomb force. The strong drive field with amplitude E_L and weak probe field with amplitude E_p are applied to drive the optical cavity. In the absence of the radiation pressure and the Coulomb force, the equilibrium separation between the charged object and the charged mechanical resonator is expressed by r_0.[42]

According to the theory of the input-output relation, $\varepsilon_T = 2\kappa\delta c_+$, the component of the output field at the probe frequency is given as

$$\varepsilon_T = 2\kappa_c \delta c_+ = \frac{2\kappa_c}{2\kappa_c - ix + \dfrac{\beta}{\dfrac{\gamma_m}{4} - ix - \dfrac{i\eta}{m\omega_m} + N}}. \tag{9}$$

The real part $\mathrm{Re}[\varepsilon_T]$ shows the absorption of output probe field, and the imaginary part $\mathrm{Im}[\varepsilon_T]$ shows the dispersion of output probe field. According to Refs. [1,2], if $N = 0$, the absorption line of the output probe field presents OMIT. With the term N, the conditions of the ideal OMIT dip can be easily obtained. Next, we will discuss the condition of ideal OMIT according to Eq. (9).

3. Results and discussion

We set $\frac{\gamma_m}{4} - ix - \frac{i\eta}{m\omega_m} + N = 0$.[1,2] After a few steps of algebra, we can get

$$x_0 = -\frac{\eta}{m\omega_m} - \frac{\omega_m \gamma_m}{4\kappa_c}, \tag{10}$$

$$\beta_0 = \frac{\gamma_m(\kappa_c^2 + \omega_m^2)}{2\kappa_c}, \tag{11}$$

where x_0 is the position of the OMIT dip.[1,2] From Eq. (10), it can be found that x_0 depends on Coulomb coupling strength η, optical cavity decay rates κ_c, and charged mechanical resonator damping rates γ_m. It is obvious that x_0 is always less than zero with Coulomb coupling strength $\eta > 0$. Given a suitable β_0 according to Eq. (11), even if the charged mechanical resonator damping rate is non-zero, the ideal OMIT can also occur.[1,2] It may be noted that $\beta > \beta_0$ indicates optomechanically induced amplification ($\mathrm{Re}[\varepsilon_T] < 0$), while $\beta = \beta_0$ represents OMIT.[1,2]

According to Eq. (11), we could investigate the ideal OMIT behaviors of the cavity optoelectromechanical system under different parameter regimes, such as the cases of the resolved sideband regime $\kappa_c < \omega_m$ and the unresolved sideband regime $\kappa_c > \omega_m$. In the calculations below, the charged mechanical resonator damping rates γ_m, and Coulomb coupling strength η are also included. The numerical results are obtained by choosing the reasonable system parameters. The γ_m is set $\gamma_m \ll \omega_m, \kappa_c$, the charged mechanical resonator damping rates $\gamma_m = 1$ Hz, resonance frequency $\omega_m = 10^4$ Hz and mass $m = 5$ g, and Coulomb coupling strength $\eta = 50$ Hz.

In Fig. 2, we present the real part $\mathrm{Re}[\varepsilon_T]$ ((a) and (c)) and the imaginary part $\mathrm{Im}[\varepsilon_T]$ ((b) and (d)) of the output probe field as a function of the normalized frequency detuning x/γ_m when $\kappa_c = 0.2\omega_m$ ((a) and (b)) and $\kappa_c = 2\omega_m$ ((c) and (d)). We first consider $\kappa_c = 0.2\omega_m$, which is shown in Figs. 2(a) and 2(b). Figure 2(a) shows that the real part can reach to the maximum value $\mathrm{Re}[\varepsilon_T] = 1$ and a single dip occurs around $x_0/\gamma_m = -2.25$, which means the typical OMIT of the output probe field. Meanwhile, the real part have a minimum value $\mathrm{Re}[\varepsilon_T] = 0$, which suggests that the ideal OMIT can be attained with the help of NRWA effect. We continue to study the case of unresolved sideband regime $\kappa_c = 2\omega_m$ in the cavity optoelectromechanical system. When the cavity optoelectromechanical system changes from $\kappa_c = 0.2\omega_m$ to $\kappa_c = 2\omega_m$, the ideal OMIT can still appear as shown in Fig. 2(c). From Figs. 2(a) and 2(c), we can conclude that just by modulating κ_c, the structure of the ideal OMIT spectral is only a transparency window, and the transparency window depth remain unchanged. It is obvious that the slope of the steep dispersion curve around frequency $-\frac{\eta}{m\omega_m\gamma_m} - \frac{\omega_m}{4\kappa_c}$ (at same frequency corresponding to ideal OMIT) is negative, which indicates that the output probe field can be appeared slow light effect from Figs. 2(b) and 2(d). More importantly, three conclusions can be drawn from Fig. 2. The first one is the different position of the ideal OMIT dip, and the dip appears at frequency $-\frac{\eta}{m\omega_m\gamma_m} - \frac{\omega_m}{4\kappa_c}$. The second one is the different width of the ideal transparency window. The third one is the different dispersion curve slope. In the following section, we will study the position of the ideal OMIT dip, the ideal transparency window width and the dispersion curve slope in cavity optoelectromechanical system by adjusting Coulomb coupling strength η, cavity decay rates κ_c, and charged mechanical resonator

damping rates γ_m.

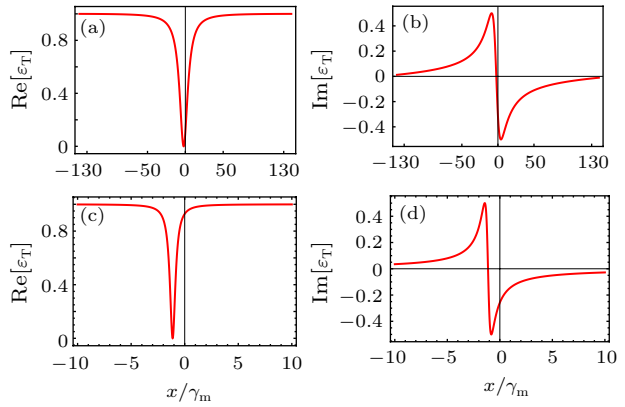


Fig. 2. The real part Re[ε_T] ((a) and (c)) and imaginary part Im[ε_T] ((b) and (d)) of the output probe field as a function of normalized frequency detuning x/γ_m in resolved sideband regime $\kappa_c = 0.2\omega_m$ ((a) and (b)) and unresolved sideband regime $\kappa_c = 2\omega_m$ ((c) and (d)).

Equation (10) shows that the Coulomb coupling strength η is the parameter that could affect the position of the ideal OMIT dip x_0. Therefore, how to modulate Coulomb coupling strength η becomes a issue. We consider the effects of the η on the ideal OMIT in the case of the resolved sideband regime $\kappa_c < \omega_m$. In Fig. 3(a), we plot the real part Re[ε_T] of the output probe field versus the normalized frequency detuning x/γ_m for the Coulomb coupling strength η in the case of resolved sideband $\kappa_c < \omega_m$. The Coulomb coupling strength η is set with different values: $\eta = \eta_0$ (red solid curve), $\eta = 8\eta_0$ (blue dashed curve), and $\eta = 100\eta_0$ (black dotted curve) with $\eta_0 = 50$ Hz. From the red solid curve, blue dashed curve and black dotted curve in Fig. 3(a), we can see that with different coupling strength η, the OMIT dip appears in different position. In the case of Coulomb coupling $\eta = \eta_0$ (red solid cure), we can get $x_0/\gamma_m = 2.25$, which is coincide with Fig. 2(a). As for the black dotted curve, we set Coulomb coupling strength $\eta = 100\eta_0$, and compared with blue dashed curve, we find the location of the ideal OMIT dip changes more obviously. So, it can be clearly seen that the dip of the ideal OMIT moves leftward with the Coulomb coupling strength η increasing. From Eq. (10), we know that if κ_c/ω_m is fixed, the location of the ideal OMIT dip x_0/γ_m decreases monotonically with Coulomb coupling strength η increasing. In Fig. 3(b), we plot the location of the ideal OMIT dip x_0/γ_m versus the Coulomb coupling strength η/η_0. The trend reflected in Fig. 3(b) indicates that the value of x_0/γ_m will definitely become smaller with increase of Coulomb coupling strength η.

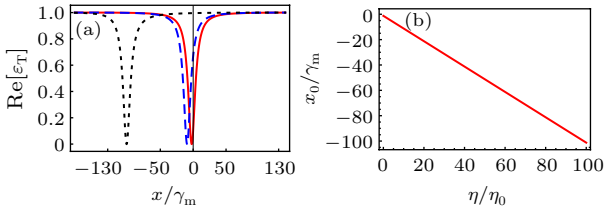


Fig. 3. (a) Real part Re[ε_T] of the output probe field versus the normalized frequency detuning x/γ_m for different values of η in the cases of resolved sideband regime $\kappa_c < \omega_m$. Here $\eta = \eta_0$ for the red solid curve, $\eta = 8\eta_0$ for the blue dashed curve, and $\eta = 100\eta_0$ for the black dotted curve. (b) The location of the OMIT dip x_0/γ_m versus the Coulomb coupling strength η/η_0. We assume that κ_c is a fixed value $\kappa_c = 0.2\omega_m$, $\eta_0 = 50$ Hz.

In the following, we can obtain the transparency window width Γ (full width at half maximum) from Eq. (9). To obtain the transparency window width Γ, we thus need to specify[1,2]

$$x = x_0 + y. \tag{12}$$

Substituting Eq. (12) into Eq. (9), we have

$$\varepsilon_T = \frac{2\kappa_c}{2\kappa_c + i\left[\dfrac{\eta}{m\omega_m} + \dfrac{\omega_m\gamma_m}{4\kappa_c} - y + \dfrac{\gamma_m(\kappa_c^2+\omega_m^2)}{2\kappa_c y}\right]}. \tag{13}$$

Setting Re[ε_T] = 0.5 , we have

$$y^2 - \left(\frac{\eta}{m\omega_m} + \frac{\omega_m\gamma_m}{4\kappa_c} \mp 2\kappa_c\right) y - \frac{\gamma_m(\kappa_c^2+\omega_m^2)}{2\kappa_c} = 0. \tag{14}$$

Equation (14) is a quadratic equation in y that will have two distinct roots y_1 and y_2,

$$y_1 = \frac{\dfrac{\eta}{m\omega_m} + \dfrac{\omega_m\gamma_m}{4\kappa_c} - 2\kappa_c + \sqrt{\left(\dfrac{\eta}{m\omega_m} + \dfrac{\omega_m\gamma_m}{4\kappa_c} - 2\kappa_c\right)^2 + \dfrac{2\gamma_m(\kappa_c^2+\omega_m^2)}{\kappa_c}}}{2},$$

$$y_2 = \frac{\dfrac{\eta}{m\omega_m} + \dfrac{\omega_m\gamma_m}{4\kappa_c} + 2\kappa_c - \sqrt{\left(\dfrac{\eta}{m\omega_m} + \dfrac{\omega_m\gamma_m}{4\kappa_c} + 2\kappa_c\right)^2 + \dfrac{2\gamma_m(\kappa_c^2+\omega_m^2)}{\kappa_c}}}{2}.$$

Then the transparency window width can be calculated by the difference between the two roots[1,2]

$$\Gamma = y_1 - y_2. \tag{15}$$

In order to get deeper insight into the transparency window width, we need to deal with Eq. (15). It is shown that under certain conditions ($\gamma_m \ll \omega_m, \kappa_c$), the complicated expression of Eq. (15) can be simplified as

$$\Gamma = \frac{2\gamma_m\omega_m^2 m^2(\kappa_c^2+\omega_m^2)}{4m^2\kappa_c^2\omega_m^2 - \eta^2}. \tag{16}$$

In Eq. (16), the transparency window width Γ will change with different γ_m, and κ_c. To see the effect of the optical cavity decay rate κ_c/ω_m and charged mechanical resonator damping rate γ_m on the transparency window width, we plot the

transparency window width Γ as functions of the decay rate of cavity κ_c/ω_m and charged mechanical resonator damping rate γ_m in Fig. 4(a) with unresolved sideband regime $\kappa_c > \omega_m$ and in Fig. 4(b) with the resolved sideband regime $\kappa_c < \omega_m$. Figures 4(a) and 4(b) show that the trend of the transparency window width Γ agrees very well for this two cases. We can obtain the following three results, the first one of which is that the larger charged mechanical resonator damping rate γ_m will induce wider transparency window, if κ_c/ω_m is fixed. Secondly, when mechanical resonator damping rate γ_m is fixed, larger κ_c leads to the decrease of the transparency window width Γ, so the transparency window becomes narrower and sharper. Thirdly, we see that the transparency window width Γ increases significantly when κ_c increases from unresolved sideband regime to resolved sideband regime. For example, we can see that the transparency window width reaches the value $\Gamma = 125$ Hz when $\kappa_c/\omega_m = 0.2$ and mechanical resonator damping rate $\gamma_m = 10$ Hz for fixed $\eta = 50$ Hz. However, under the same conditions, except $\kappa_c/\omega_m = 1.5$, the transparency window width reaches to the value of $\Gamma = 10$ Hz. We need to emphasize that although the transparency window becomes narrower and sharper with larger κ_c, the depth of the transparency windows remain unchanged.

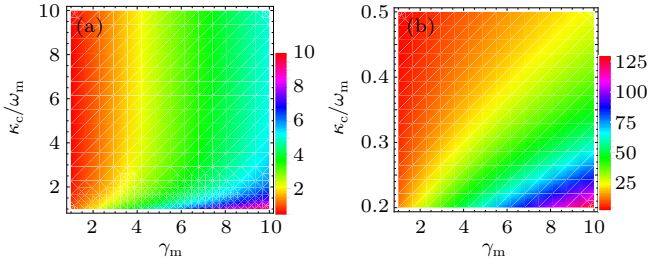


Fig. 4. The transparency window width Γ plotted as function of the cavity decay rate κ_c/ω_m and charged mechanical resonator damping γ_m. (a) The unresolved sideband regime $\kappa_c > \omega_m$ and (b) resolved sideband regime $\kappa_c < \omega_m$.

Besides of the manipulation of $\mathrm{Re}[\varepsilon_T]$ by κ_c, $\mathrm{Im}[\varepsilon_T]$ can also be affected by κ_c. From Eq. (13), we can get $\mathrm{Im}[\varepsilon_T]$ and further calculate the dispersion curve slope $K = \partial\,\mathrm{Im}[\varepsilon_T]/\partial y$,[1,2] so we obtain the following equation:

$$K = \frac{\left(\kappa_c^2\gamma_m y+\gamma_m\omega_m^2 y+\frac{2\eta\kappa_c}{m\omega_m}y^2+\frac{\gamma_m\omega_m}{2}y^2-2y^3\kappa_c\right)\left[8\kappa_c^2 y+\left(\frac{2\eta}{m\omega_m}+\frac{\gamma_m\omega_m}{2\kappa_c}-4y\right)\left(\frac{\gamma_m\kappa_c^2+\gamma_m\omega_m^2}{2\kappa_c}+\frac{\eta}{m\omega_m}y+\frac{\gamma_m\omega_m}{4\kappa_c}y-y^2\right)\right]}{\left[4\kappa_c^2y^2+\left(\frac{\gamma_m\kappa_c^2+\gamma_m\omega_m^2}{2\kappa_c}+\frac{\eta}{m\omega_m}y+\frac{\gamma_m\omega_m}{4\kappa_c}y-y^2\right)^2\right]^2}$$
$$-\frac{\left(\frac{\gamma_m\kappa_c^2+\gamma_m\omega_m^2}{\kappa_c}+\frac{4\eta}{m\omega_m}y+\frac{\gamma_m\omega_m}{\kappa_c}y-6y^2\right)\kappa_c}{4\kappa_c^2y^2+\left(\frac{\gamma_m\kappa_c^2+\gamma_m\omega_m^2}{2\kappa_c}+\frac{\eta}{m\omega_m}y+\frac{\gamma_m\omega_m}{4\kappa_c}y-y^2\right)^2}. \tag{17}$$

It can be seen that the form of Eq. (17) is somewhat complicated. According to Eq. (17), the maximum dispersion curve slope is given by

$$K_{max} = -\frac{4\kappa_c^2}{\gamma_m(\kappa_c^2+\omega_m^2)}, \tag{18}$$

with $y = 0$. In Eq. (18), κ_c and γ_m play important roles. In addition, K_{max} is immune to Coulomb coupling strength η.

We want to investigate the effect of κ_c on K_{max}. So, we plot K_{max} varies versus κ_c/ω_m, with $\gamma_m = 1$ Hz (red solid line), $\gamma_m = 0.7$ Hz (blue dashed line), and $\gamma_m = 0.4$ Hz (black dotted curve), in Fig. 5. As depicted clearly in Fig. 5, with the increase of κ_c/ω_m, the dispersion curve slope K_{max} reduces significantly at first, which means that the narrow transparency dip deepens. That is to say, the ideal OMIT effect is enhanced, however, while further strengthening κ_c/ω_m, the maximum dispersion curve slope K_{max} starts to be stable. Meanwhile, the curve with $\gamma_m = 1$ Hz (red solid line) is much steeper than that with $\gamma_m = 0.7$ Hz (blue dashed line). The steeper the slope of dispersion curve is, the more significant the slow light effect becomes.

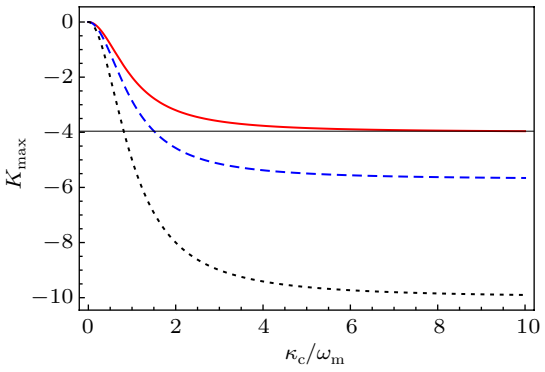


Fig. 5. The dispersion curve slope K_{max} as a function of the charged mechanical resonator damping κ_c/ω_m, with $\gamma_m = 1$ Hz (red solid line), $\gamma_m = 0.7$ Hz (blue dashed line), and $\gamma_m = 0.4$ Hz (black dotted curve).

4. Conclusions

The aim of the present work is to investigate the ideal OMIT properties in a cavity optoelectromechanical system driven by strong pump field and weak probe field. The charged mechanical resonator is simultaneously coupled to the optical cavity via radiation pressure and to the adjoining charged object via the Coulomb force. Solving the quantum Langevin

equations for the cavity optoelectromechanical system operators and using the input-output relation of the cavity, we derive an analytical expression for the output probe field. Although the charged mechanical resonator damping rate is nonzero, the ideal OMIT can still appear when we apply the non-rotating wave approximation effect. In addition, we analyze the effects of the Coulomb coupling strength, optical cavity decay rate, and charged mechanical resonator damping rate on the ideal OMIT.

Appendix A: Derivation of δc_+ with rotating wave approximation

We introduce the annihilation (creation) operator b ($b^\dagger$) of the charged mechanical resonator, and have $q = (\frac{\hbar}{2m\omega_{\rm m}})^{1/2}(b^\dagger + b)$ and $p = {\rm i}(\frac{\hbar m\omega_{\rm m}}{2})^{1/2}(b^\dagger - b)$. The Hamiltonian in Eq. (1) can be presented as below:

$$H = \hbar\Delta_{\rm c}c^\dagger c + \hbar(\omega_{\rm m} - 2G)b^\dagger b - \hbar g c^\dagger c(b^\dagger + b) - \hbar G(b^{\dagger 2} + b^2) + {\rm i}\hbar E_{\rm L}(c^\dagger - c) + {\rm i}\hbar(E_{\rm p}c^\dagger {\rm e}^{-{\rm i}\delta t} - E_{\rm p}^* c\,{\rm e}^{{\rm i}\delta t}), \tag{A1}$$

where $G = \frac{\eta}{2m\omega_{\rm m}}$. The Langevin equations of the cavity optoelectromechanical system operators can be described as below:

$$\begin{aligned}\dot{b} &= -\frac{\gamma_{\rm m}}{2}b - {\rm i}\omega_{\rm m}b + {\rm i}gc^\dagger c + 2{\rm i}G(b^\dagger + b),\\ \dot{c} &= -2\kappa_{\rm c}c - {\rm i}\Delta_{\rm c}c + {\rm i}gc(b^\dagger + b) + E_{\rm L} + E_{\rm p}\,{\rm e}^{-{\rm i}\delta t}.\end{aligned} \tag{A2}$$

The operator can be written as the steady-state mean value plusing its small fluctuation $A = A_{\rm s} + \delta A$. Substituting it into Eq. (A2), we can get steady state solutions $c_{\rm s} = \frac{E_{\rm L}}{2\kappa_{\rm c} + {\rm i}\Delta}$, where $\Delta = \omega_{\rm c} - \omega_{\rm L} - g(b_{\rm s}^* + b_{\rm s})$. And then the Langevin equations of the fluctuation operators can be described as below:

$$\begin{aligned}\delta\dot{b} &= -\frac{\gamma_{\rm m}}{2}\delta b - {\rm i}\omega_{\rm m}\delta b + {\rm i}g(\delta c^* c_{\rm s} + c_{\rm s}^*\delta c) + 2{\rm i}G(\delta b^* + \delta b),\\ \delta\dot{c} &= -2\kappa_{\rm c}\delta c - {\rm i}\Delta\delta c + {\rm i}gc_{\rm s}(\delta b^* + \delta b) + E_{\rm p}\,{\rm e}^{-{\rm i}\delta t}.\end{aligned} \tag{A3}$$

Now let us use non-rotating wave approximation to solve Eq. (A3). We assume that the fluctuation term δA has the following form:

$$\delta A = E_{\rm p}\delta A_+\,{\rm e}^{-{\rm i}\delta t} + E_{\rm p}^*\delta A_-\,{\rm e}^{{\rm i}\delta t}. \tag{A4}$$

Substituting Eq. (A4) into Eq. (A3), we can get

$$\delta c_+ = \frac{1}{2\kappa_{\rm c} - {\rm i}x + \dfrac{\beta'}{\dfrac{\gamma_{\rm m}}{2} - {\rm i}x - 2{\rm i}G + N'}}, \tag{A5}$$

where $\beta' = g^2|c_{\rm s}|^2$ and NRWA effect term $N' = -\frac{\beta}{2\kappa_{\rm c} - 2{\rm i}\omega_{\rm m}}$.

Now we will apply the rotating wave approximation (neglecting the counter-rotating terms) to solve Eq. (A3) to find out the origin of N'. Considering the cavity that is driven by a coupling field at the mechanical red sideband $\Delta \simeq \omega_{\rm m}$ and with the formation of solution of Eq. (A3) in the following form $\delta b = \delta b\,{\rm e}^{-{\rm i}\omega_{\rm m}t}$, $\delta c = \delta c\,{\rm e}^{-{\rm i}\Delta t}$, we obtain the following equations:

$$\begin{aligned}\delta\dot{b} &= -\frac{\gamma_{\rm m}}{2}\delta b + {\rm i}gc_{\rm s}^*\delta c + 2{\rm i}G\delta b,\\ \delta\dot{c} &= -2\kappa_{\rm c}\delta c + {\rm i}gc_{\rm s}\delta b + E_{\rm p}\,{\rm e}^{-{\rm i}(\delta - \omega_{\rm m})t}.\end{aligned} \tag{A6}$$

We introduce the reverse substitutions $\delta b = \delta b\,{\rm e}^{{\rm i}\omega_{\rm m}t}$, and $\delta c = \delta c\,{\rm e}^{{\rm i}\omega_{\rm m}t}$. Substituting them into Eq. (A6), we obtain the following equations:

$$\begin{aligned}\delta\dot{b} &= -\left(\frac{\gamma_{\rm m}}{2} + {\rm i}\omega_{\rm m}\right)\delta b + {\rm i}gc_{\rm s}^*\delta c + 2{\rm i}G\delta b,\\ \delta\dot{c} &= -(2\kappa_{\rm c} + {\rm i}\omega_{\rm m})\delta c + {\rm i}gc_{\rm s}\delta b + E_{\rm p}\,{\rm e}^{-{\rm i}\delta t}.\end{aligned} \tag{A7}$$

Substituting Eq. (A4) into Eq. (A7), we can get

$$\delta c_+ = \frac{1}{2\kappa_{\rm c} - {\rm i}x + \dfrac{\beta'}{\dfrac{\gamma_{\rm m}}{2} - {\rm i}x - 2{\rm i}G}}. \tag{A8}$$

The term N' does not appear in Eq. (A8). It is clear that the origin of the term N' in Eq. (A5) is the NRWA effect.

References

[1] Yan X B 2020 *Phys. Rev. A* **101** 043820
[2] Yan X B 2021 *J. Phys. B* **54** 035401
[3] Yan X B 2021 *Physica E* **131** 114759
[4] Agarwal G S and Huang S M 2010 *Phys. Rev. A* **81** 041803
[5] Weis S, Rivière R, Deleglise S, Gavartin E, Arcizet O, Schliesser A and Kippenberg T J 2011 *Science* **330** 1520
[6] He B, Yang L and Jiang X S 2018 *Phys. Rev. Lett.* **120** 203904
[7] Yan X B, Cui C L, Gu K H, Tian X D, Fu C B and Wu J H 2014 *Opt. Express* **22** 4886
[8] Yan X B, Deng Z J, Tian X D and Wu J H 2019 *Opt. Express* **27** 24393
[9] Guo Y J, Li K, Nie W J and Li Y 2014 *Phys. Rev. A* **90** 053841
[10] Wang J 2021 *Chin. Phys. B* **30** 024204
[11] Wang J 2014 *Acta Optica Sinica* **40** 1827001
[12] Hou B P, Wei L F and Wang S J 2015 *Phys. Rev. A* **92** 033829
[13] Yang Q, Hou B P and Lai D G 2017 *Opt. Express* **25** 9697
[14] Wang T, Zheng M H, Bai C H, Wang D Y, Zhu A D, Wang H F and Zhang S 2018 *Ann. Phys.* **530** 1800228
[15] Ullah K, Jing H and Saif F 2018 *Phys. Rev. A* **97** 033812
[16] Gu K H, Yan X B, Zhang Y, Fu C B, Liu Y M, Wang X and Wu J H 2015 *Opt. Commun* **338** 569
[17] Lü H, Wang C Q, Yang L and Jing H 2018 *Phys. Rev. Appl.* **10** 014006
[18] Zhang H, Saif F, Jiao Y and Jing H 2018 *Opt. Express* **26** 25199
[19] Jiao Y F, Lu T X and Jing H 2018 *Phys. Rev. A* **97** 013843
[20] Xiong H, Huang Y M, Wan L L and Wu Y 2016 *Phys. Rev. A* **94** 013816
[21] Xiao R J, Pan G X and Zhou L 2015 *Int. J. Theor. Phys.* **54** 3665
[22] Kong C, Li S, You C, Xiong H and Wu Y 2018 *Sci. Rep.* **8** 1060
[23] Xu X W, Song L N, Zheng Q, Wang Z H and Li Y 2018 *Phys. Rev. A* **98** 063845
[24] Chen B, Jiang C and Zhu K D 2011 *Phys. Rev. A* **83** 055803
[25] Liu Y C, Li B B and Xiao Y F 2017 *Nanophotonics* **6** 789
[26] Aspelmeyer M, Kippenberg T J and Marquardt F 2014 *Rev. Mod. Phys.* **86** 1391
[27] Kippenberg T J and Vahala K J 2007 *Opt. Express* **15** 17172
[28] Xiong H and Wu Y 2018 *Appl. Phys. Rev.* **5** 031305
[29] Gao Y P, Wang T J, Cao C, Mi S C, Yang D, Zhang Y and Wang C 2017 *IEEE Photon. J.* **9** 6800411
[30] Xiong H, Si L G, Lv X Y, Yang X X and Wu Y 2015 *Sci. China Phys. Mech. Astron.* **58** 1
[31] Cao C, Mi S C, Gao Y P, He L Y, Yang D, Wang T J, Zhang R and Wang C 2016 *Sci. Rep.* **6** 22920
[32] Cao C, Mi S C, Wang T J, Zhang R and Wang C 2016 *IEEE J. Quantum Electron.* **52** 7000205
[33] Cao C, Chen X, Duan Y W, Fan L, Zhang R, Wang T J and Wang C 2017 *Optik* **130** 659
[34] Xiong X R, Gao Y P, Liu X F, Cao C, Wang T J and Wang C 2018 *Sci. China: Phys., Mech. Astron.* **61** 90322

[35] Wu S C, Qin L G, Lu J and Wang Z Y 2019 *Chin. Phys. B* **28** 074204
[36] Gu K H, Yan D, Zhang M L, Yin J Z and Fu C B 2019 *Acta Phys. Sin.* **68** 54201 (in Chinese)
[37] Li S, Li H Z, Xu J P, Zhu C J and Yang Y P 2019 *Acta Phys. Sin.* **68** 174202 (in Chinese)
[38] Liu N, Huang S, Li J Q and Liang J Q 2019 *Acta Phys. Sin.* **68** 193701 (in Chinese)
[39] Bai C H, Wang D Y, Zhang S, Liu S T and Wang H F 2021 *Phys. Rev. A* **103** 033508
[40] Wang J, Tian X D, Liu Y M, Cui C L and Wu J H 2018 *Laser Phys.* **28** 065202
[41] Ma P C, Zhang J Q, Xiao Y, Feng M and Zhang Z M 2014 *Phys. Rev. A* **90** 043825
[42] Zhang J Q, Li Y, Feng M and Xu Y 2012 *Phys. Rev. A* **86** 053806
[43] Chen B, Wang L D, Zhang J, Zhai A P and Xue H B 2016 *Phys. Lett. A* **380** 798
[44] Hu C S, Huang X R, Shen L T, Yang Z B and Wu H Z 2017 *Eur. Phys. J. D* **71** 24
[45] Wang J 2020 *Chin. Phys. B* **29** 034210
[46] Jiang C, Song L N and Li Y 2018 *Phys. Rev. A* **97** 053812
[47] Qin G Q, Yang H, Mao Xuan, Wen J W, Wang M, Ruan D and Long G L 2020 *Opt. Express* **28** 580